

Power balance analysis at the L-H transition in JET-ILW NBI-heated deuterium plasmas

P. Vincenzi^{1,2}, E. R. Solano³, E. Delabie⁴, C. Bourdelle⁵, G. Snoep⁶, A. Baciero³, G. Birkenmeier⁷, P. Carvalho⁹, M. Cavedon⁸, M. Chernyshova¹⁰, J. Citrin⁶, J.M. Fontdecaba³, J.C. Hillesheim¹¹, A. Huber¹², C. Maggi¹¹, S. Menmuir¹¹, F. I. Parra¹³ and JET Contributors*

¹Consorzio RFX, Padova, Italy

²Institute for Plasma Science and Technology, National Research Council, 35127 Padova, Italy

³Laboratorio Nacional de Fusión, CIEMAT, Madrid, Spain

⁴Oak Ridge National Laboratory, Oak Ridge, TN 37831-6169, TN, United States of America

⁵CEA, IRFM, F-13108 Saint Paul Lez Durance, France

⁶FOM Institute DIFFER, Eindhoven, Netherlands

⁷Max-Planck-Institut für Plasmaphysik, D-85748 Garching, Germany

⁸Dipartimento di Fisica, Università di Milano-Bicocca, 20126 Milan, Italy

⁹Instituto de Plasmas e Fusão Nuclear, Instituto Superior Técnico, Universidade de Lisboa, Portugal

¹⁰Institute of Plasma Physics and Laser Microfusion, Hery 23, 01-497 Warsaw, Poland

¹¹CCFE, Culham Science Centre, Abingdon, Oxon, OX14 3DB, United Kingdom of Great Britain and Northern Ireland

¹²Forschungszentrum Jülich GmbH, Institut für Energie- und Klimaforschung, Plasmaphysik, 52425 Jülich, Germany

¹³Rudolf Peierls Centre for Theoretical Physics, University of Oxford, Oxford OX1 3PU, United Kingdom of Great Britain and Northern Ireland

*See the author list of *J. Mailloux et al 2022 Nucl. Fusion 62 042026*

E-mail: pietro.vincenzi@igi.cnr.it

Abstract

The understanding of the physics underlying the L-H transition has strong implications for ITER and DEMO. In many tokamaks, including JET, it has been observed that, at a particular plasma density, $n_{e,\min}$, the power necessary to access H-mode P_{L-H} is minimum. In the present work, L-H transitions of JET deuterium plasmas heated by neutral beam injection (NBI) are studied for the first time by means of a power balance analysis to characterize the main contributions in the transition, through integrated transport modelling. In the pulses analysed, we do observe a minimum of the L-H power threshold in density, indicating the presence of density branches and of $n_{e,\min}$. Electron and ion heat fluxes at the transition are estimated separately. The electron/ion equipartition power results to be in favour of the ions, as shown by QuaLiKiz quasilinear gyrokinetic simulations, which predict a larger ion transport that causes $T_e > T_i$. The resulting edge ion heat flux also shows a clear change of slope below $n_{e,\min}$, similarly to ASDEX-Upgrade NBI pulses [Ryter F. et al 2014 Nucl. Fusion 54 083003]. JET NBI data are compared to radio-frequency heated ASDEX-Upgrade and Alcator C-mod pulses [Schmidtmayr M. et al 2018 Nucl. Fusion 58 056003], showing a different trend of the power coupled to ions at the L-H transition with respect to the linearity observed in the radio-frequency heated plasmas. The presence of $n_{e,\min}$ and the role of the ion heat flux is discussed in the paper, although it seems not possible to explain the presence of a P_{L-H} minimum in density by a critical ion heat flux and by the equipartition power for the JET NBI-heated plasmas analysed.

Keywords: L-H, H-mode, power balance analysis, ion heat flux, JET

1. Introduction

High energy and particle confinement regime, H-mode, is achieved when enough power is coupled to the plasma, as already noted in 1982 in the ASDEX tokamak [1]. The transition from low confinement, L-mode, to H-mode (L-H transition) happens at a certain power threshold, which depends on plasma density. It is possible to classify L-H transitions in two branches: the first, at higher density, is characterized by a power threshold P_{L-H} which increases monotonically with density (the so-called high density branch). The most complete empirical scaling law for the high density branch (to which we will refer to as ‘‘ITPA 2008 scaling’’ [2]) has been derived from C-wall tokamaks (except for data from Alcator C-mod tokamak [3] equipped with a full metal –molybdenum- wall) and presents explicit toroidal magnetic field dependence. It yields:

$$P_{L-H}[\text{MW}] = 0.049 \bar{n}_e^{0.72} B_T^{0.8} S^{0.94} \quad (\text{eq. 1})$$

with line averaged electron density \bar{n}_e in 10^{20} m^{-3} , toroidal magnetic field B_T in T and the plasma surface S in m^2 . The high density branch was observed in all tokamaks since the very first studies on P_{L-H} scaling laws [4], [5], [6], [7]. Subsequent studies showed that P_{L-H} often exhibits a minimum, or at least a flattening, as the L-mode plasma target density decreases, at a corresponding density called ‘‘minimum density’’, $n_{e,\text{min}}$. At densities lower than $n_{e,\text{min}}$, in some cases, the power threshold is found to increase when decreasing further the density, phenomenon that characterizes the second branch, i.e. the so called ‘‘low density branch’’. Although reported in many devices [7], [8], [9], [10], [11], [12] the observation of the low-density branch is not universal. For instance, concerning JET tokamak [13], in previous Carbon-wall plasmas the rollover of the power threshold at low density was not observed in all divertor geometries; it reappeared only with the installation of the JET ITER-like wall (ILW) [14]. In JET, both the power threshold and the value of $n_{e,\text{min}}$ (when observed) depend on the toroidal magnetic field and plasma shape, as first reported in [15] and subsequently confirmed in [12], [14]. As observed in various other devices, $n_{e,\text{min}}$ is also affected by plasma current. Various investigations of P_{L-H} dependency on target density have been carried out in JET since the installation of the ITER-like wall [14], [16]. For the same boundary conditions (shape, current, field, auxiliary heating), the value of $n_{e,\text{min}}$ showed a clear dependence on plasma isotope, being considerably higher in hydrogen plasmas compared to deuterium plasmas [17], [18]. Recent results at JET indicate that $n_{e,\text{min}}$ in tritium plasmas could be lower than for D, while He plasmas show a $n_{e,\text{min}}$ higher than H, both of them higher than in D [19]. The understanding of the L-H transition physics and consequently of the existence of a minimum in density is fundamental also for future experiment and reactors. JET studies have therefore a strong implication for ITER H-mode access [20], in particular since the installation of the metallic, ITER-like, first wall. It also impacts the design of EU DEMO, where the L-H transition, if happening before the alpha-dominated phase, would rely mainly on auxiliary heating systems which must be dimensioned accordingly [21].

In this context, experiments were conducted in the last years at JET aimed at characterizing the L-H transition and understanding the underlying physics. The current paper presents the first detailed power balance analysis of JET L-H transitions for a subset of D plasmas heated by neutral beam injection (NBI), decoupling all the power terms contributing to P_{L-H} , separating the electron and ion channels. The scope of the work is to investigate power contributions to JET L-H transitions exploiting experimental data interpretation and transport modelling, and to discuss the role of the different terms, in particular of the edge ion heat flux. We also aim to compare our data to the proposed models based on ASDEX-Upgrade (AUG) and Alcator C-mod (briefly ‘‘C-mod’’) experiments.

The paper is organized as follows. The description of the database selected and the L-H transition identification is presented in sec. 2. In sec. 3, the power balance analysis is illustrated, with particular attention to the estimation of the various power terms and their uncertainties. JET results are then compared in sec. 4 with models proposed on the base of AUG and C-mod results. The paper ends with a conclusion and outlook.

2. L-H transition threshold identification

The data selected for the analysis comes from a set of NBI-heated, deuterium plasmas where the target plasma density was varied [19], [22], [23], [24]. The scan in density (see e.g. figure 1) is necessary to characterize the density branches and to identify the presence of $n_{e,\text{min}}$. Therefore, pulses used in this study were carried out at the same magnetic field, plasma current and shape, while feed-back controlled plasma density in L-mode was varied shot to shot. The plasmas had high toroidal magnetic field, $B_{\text{tor}} = 3 \text{ T}$, low triangularity δ and plasma current $I_p = 2.5 \text{ MA}$. The plasma shape in the divertor region corresponded to the so-called ‘‘horizontal target’’ configuration, where the outer strike point is in a tilted, almost horizontal, divertor tile and the inner one is on the vertical target. This set of data will be labelled as ‘‘JET NBI HT, low δ ’’ when compared to other data afterwards in the paper. Effective charge Z_{eff} was within 1.2 and 1.4. NBI was used to access H-mode, guaranteeing a relevant amount of ion heating power and main ion temperature, T_i , measurements. No other auxiliary

heating system was used. As usual in JET, the $\vec{B} \times \nabla B$ drift was directed towards the X-point, at the lower part of the vacuum chamber.

The relevant quantity to measure the L-H power threshold is P_{loss} , defined as:

$$P_{\text{loss}} = P_{\text{aux}} + P_{\text{ohm}} - \frac{dW}{dt} \quad (\text{eq. 2})$$

$$P_{\text{L-H}} = P_{\text{loss}}(t = t_{\text{L-H}})$$

where P_{aux} is the auxiliary heating power (from NBI, in our case, i.e. $P_{\text{aux}} = P_{\text{NBI}}$), P_{ohm} the ohmic power, and dW/dt the time derivative of the plasma energy content, to be taken into account for plasmas not in steady state conditions (e.g. in the dynamic phase of the access to H-mode). When we consider P_{loss} at the L-H transition time we simply speak of $P_{\text{L-H}}$. Fig. 1 represents $P_{\text{L-H}}$ as a function of density for pulses of the present dataset. Considering the complete dataset (empty and filled points of fig. 1), it is possible to identify the region of the low density branch, $n_{e,\text{min}}$ and of the high-density branch. The plasmas analysed in this work are represented by filled green circles in fig. 1 and are chosen to include the $n_{e,\text{min}}$ region between density branches. We have also reported the ITPA 2008 scaling, which results in an over-prediction in the high-density branch, as already seen for JET metallic wall experiments [25].

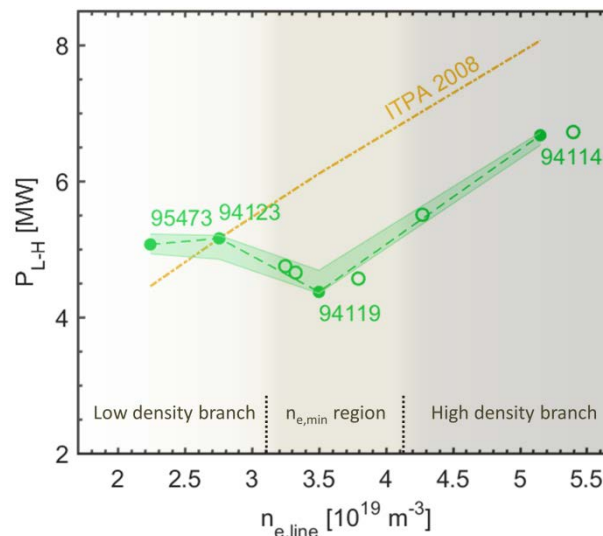


Figure 1: L-H power threshold $P_{\text{L-H}}$ as function of line averaged density for JET-ILW NBI-heated D plasmas. The plasmas represented by filled circles (pulse numbers are represented too) are analysed in the present work, although we used the entire set to identify density branches. ITPA 2008 scaling for $P_{\text{L-H}}$ in the high-density branch (eq. 1) is also reported.

In this analysis, it is important to choose the temporal interval judiciously. The L-H transition is commonly identified as the time when edge density and/or temperature rises, while simultaneously the D_α emission from the divertor drops, and consequently the plasma stays in H-mode. Fig. 2 reports the time traces in a time interval that includes the identified L-H transition time used in our analysis. If we zoom into the various transition time-windows, we often see more complex structures: dithering L-H transitions, M-modes [26], divertor oscillations, subtle transitions, etc. For JET L-H transition power threshold studies, the L-H transition time is defined as the time when the dithers end and the plasma stays in H-mode. But for the purposes of our study we find that dithers can perturb the interpretation of the profile measurements, which continue to evolve. Therefore the profiles are characterized, at low density, at the last L-mode time before the plasma stays continuously in H-mode, while, at medium and high density, at the last L-mode before the first L-H dither takes place, consistently with other JET studies, e.g. [19], [27]. In terms of power threshold, these choices do not impact on the observed minimum in $P_{\text{L-H}}$ at $n_{e,\text{min}}$. For instance, P_{loss} for pulse 94119 is very similar before and after dithering phase (fig. 2). It is possible to observe the typical and complex dynamics of L-H transitions at different plasma densities, with phenomena described in details in e.g. [27]. Plasma density clearly affects both the transition behaviour, such as the drop of D_α emission or the transition velocity, and the required power necessary to enter the H-mode with a visible change of slope passing through the density branches. In the low density branch, the L-H transition time identification is often subtle. Sometimes various L-H-L transitions take place during the power ramp, often transient M-mode phases are observed to follow sawteeth. Each sawtooth can produce a brief H-mode, which is then often quickly lost. Pulse 95473 is indeed affected by sawteeth. In this case we cannot resolve clearly in fig. 2 a rise in $n_{e,\text{edge}}$ at $t_{\text{L-H}}$, although we can still observe a slight increase in $n_{e,\text{edge}}$ just before $t = 13\text{s}$, accompanied by an increase of the edge T_e . In the low density branch, the fraction of radiated power results to

be higher than on the high density branch, likely due to a larger amount of W impurity fraction, lowering the electron temperature. Nevertheless, the power ramp and the brief H-modes conspire to slowly increase the edge n_e and T_e , until eventually the plasma stays in H-mode. By contrast, near $n_{e,\min}$ and in the high density branch, it is common to observe dithers between L and H mode. During the dithers, n_e (and sometimes T_e) can continue to increase.

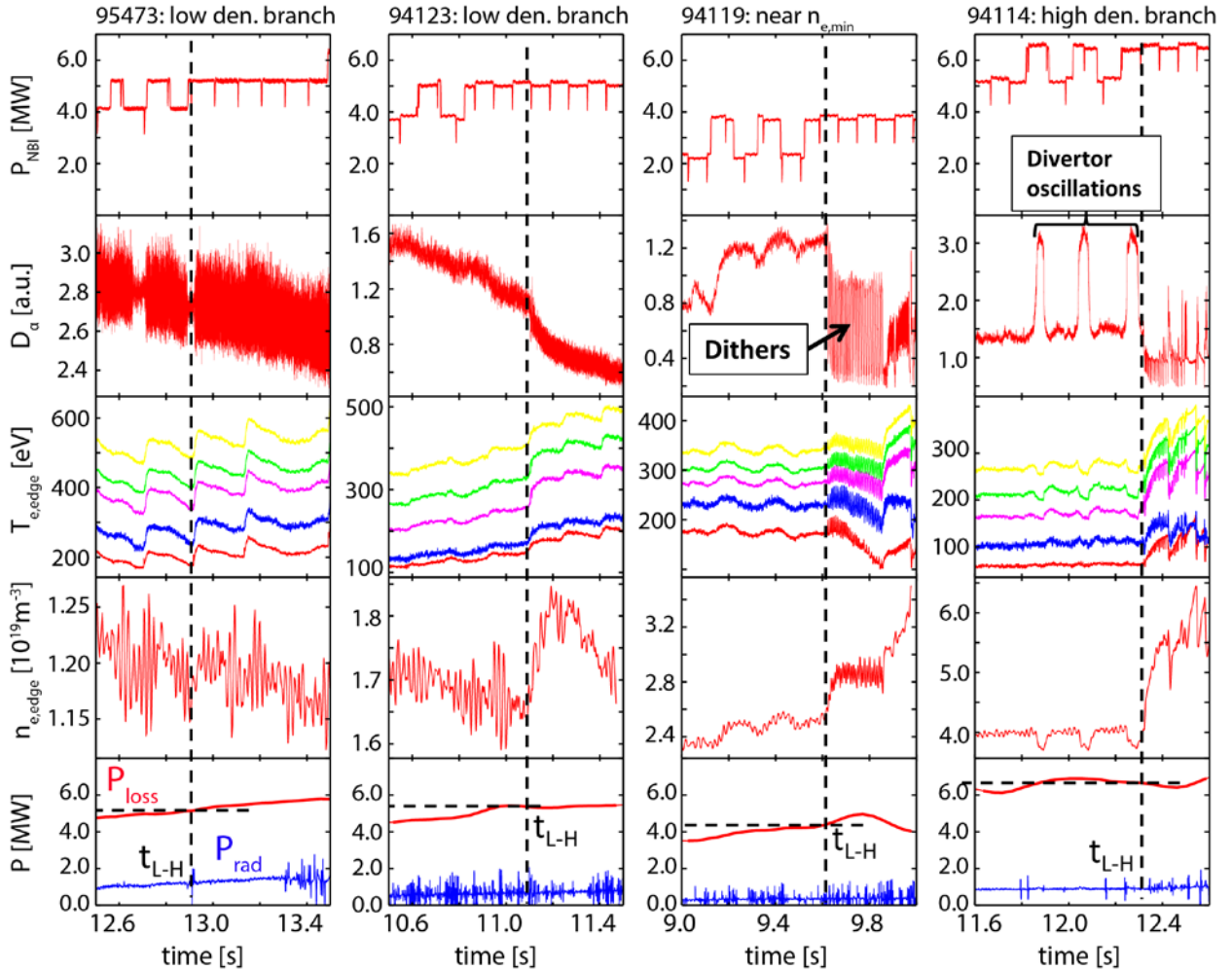


Figure 2: Time traces for L-H transition identification. From top: NBI power, D_α light emission, T_e from different edge ECE lines of sight, line-integrated pedestal density measured with a vertical interferometer line that crosses the plasma edge region, and finally radiation power P_{rad} and P_{loss} terms.

Experimental conditions are fundamental to minimize parameter uncertainties. The high toroidal magnetic field used in these experiments implies a high L-H power threshold in order to enable precise measurements of all the relevant terms. Slow power ramps ($\sim 1\text{MW/s}$) were employed, in order to better identify the L-H transition instant and the corresponding power threshold. This makes dW/dt term always negligible in our analysis with respect to plasma heating power terms (see next section for details). If NBI modulation is used to vary the heating power, as in most of the cases analysed (see fig. 2), the uncertainty on P_{loss} is difficult to be assessed precisely, since it depends on the slowing down time of the fast ions with respect to the power modulation frequency. For P_{loss} uncertainty estimation for the sub-set of pulses analysed, we decided to report the range of variation of P_{loss} signal within $t_{\text{L-H}} \pm 100$ ms: this is pictured in fig. 1 through shaded error bands. Consequently to the choice of slow power ramps, the uncertainty on P_{loss} results then rather small.

3. Ion and electron power balance analysis

We now present the estimation of all power terms contributing to P_{loss} (eq. 2) at the L-H transition, separating ion (Q_i) and electron (Q_e) surface-integrated heat fluxes:

$$P_{loss} = Q_i + Q_e$$

$$Q_i = P_{aux,i} + P_{ei} - \frac{dW_i}{dt} \quad (\text{eq. 3})$$

$$Q_e = P_{aux,e} + P_{ohm} - P_{ei} - \frac{dW_e}{dt} \quad (\text{eq. 4})$$

where P_{ei} is the electron-ion equipartition power, while the other terms have been described in sec. 2 with the difference that here are separated into ion and electron channels. P_{ei} is proportional to the volume integral of $n_e n_i (T_e - T_i) / T_e^{3/2}$, and takes into account all the plasma ion species. It is therefore positive for $T_e > T_i$, and it is subtracted to the power carried by electrons, while it is added to the power carried by ions. To estimate P_{ei} , plasma kinetic profiles are required. Electron temperature was measured by Electron Cyclotron Emission (ECE) [28] and High Resolution Thomson Scattering ‘‘HRTS’’ [29], [30] diagnostics. Edge T_i measurements were available by Charge-Exchange (CX) spectroscopy [31]. Recent improvement of main-ion CX spectroscopy diagnostic [32] allowed T_i measurements in plasma core. Temperature profiles considered for the analysis are shown in fig. 3. Plasma density was measured by HRTS and reflectometry [33], being constrained in the Scrape-off Layer (SOL) by Li-beam measurements [34], [35]. The variety of the available diagnostics implies that measurement mapping plays an important role in data interpretation. Measurements are mapped to the outer equator and fitted with appropriate functions: modified hyperbolic tangent for density profiles, polynomial or spline fits for the temperature profiles. Since the contribution of P_{ei} can be calculated with sufficient accuracy only if $(T_e - T_i)$ is larger than experimental uncertainties, we decided to integrate P_{ei} up to $\rho_{tor} = 0.85$ (being ρ_{tor} the square root of the normalized toroidal flux, $\rho_{tor} = 1$ at the Last Closed Flux Surface LCFS), assuming $P_{ei} \approx 0$ for $\rho_{tor} > 0.85$, since the measured T_e are almost equal to the measured T_i within the error bars (see fig. 3). The auxiliary power, from NBI in our case, is estimated by transport modelling. To this purpose, time-dependent, interpretative transport simulations have been carried out by the JETTO code [36] within the JINTRAC suite [37], taking as input the kinetic profiles from measurements. The simulations consider ~ 1 s before the L-H transition, in order to simulate multiple confinement times, which is in the order of 0.1 s for the energy confinement time. NBI power deposition is obtained specifically by the orbit following ASCOT Monte Carlo code [38]. Fast ion slowing down time is of the order of 100 ms or less, shorter than the considered simulation time interval. ASCOT modelling allows a correct estimation of the NBI power coupled to the plasma, by subtracting fast particle losses to the input power. At L-H transition, NBI power coupled to the plasma varies between 3 and 7 MW, of which the power coupled to plasma ions $P_{NBI,i}$ is in the range of 40-70%. The Bremsstrahlung diagnostic [39] is used for the Z_{eff} estimation. Equilibrium reconstruction is routinely produced with the EFIT code [40], constrained by the measured plasma pressure assuming $T_i = T_e$, to improve plasma equilibrium calculation with respect to the use of magnetic measurements only. The time derivative of the plasma energy content, dW/dt , both for ions and electrons, is calculated as an average over 70 ms before L-H transition. We also define the power crossing the separatrix, i.e. crossing the LCFS, as $P_{sep} = P_{L-H} - P_{rad}$, with P_{rad} the bulk radiated power. P_{sep} is sometimes used in place of P_{loss} for P_{L-H} comparisons, especially for highly radiating plasmas, and we will report it throughout the paper. For JET-ILW plasmas, the radiation level was measured with tomographic inversion of bolometry measurements [41], [42]. The resolution of bolometer channels at the edge of the plasma was insufficient to distinguish radiation close to the LCFS from SOL radiation. Consequently, we decided to take into account the reconstructed radiation profiles up to $\rho_{tor} = 0.95$ when calculating P_{rad} term. Uncertainties in radiated power density are typically of the order of 10% or less.

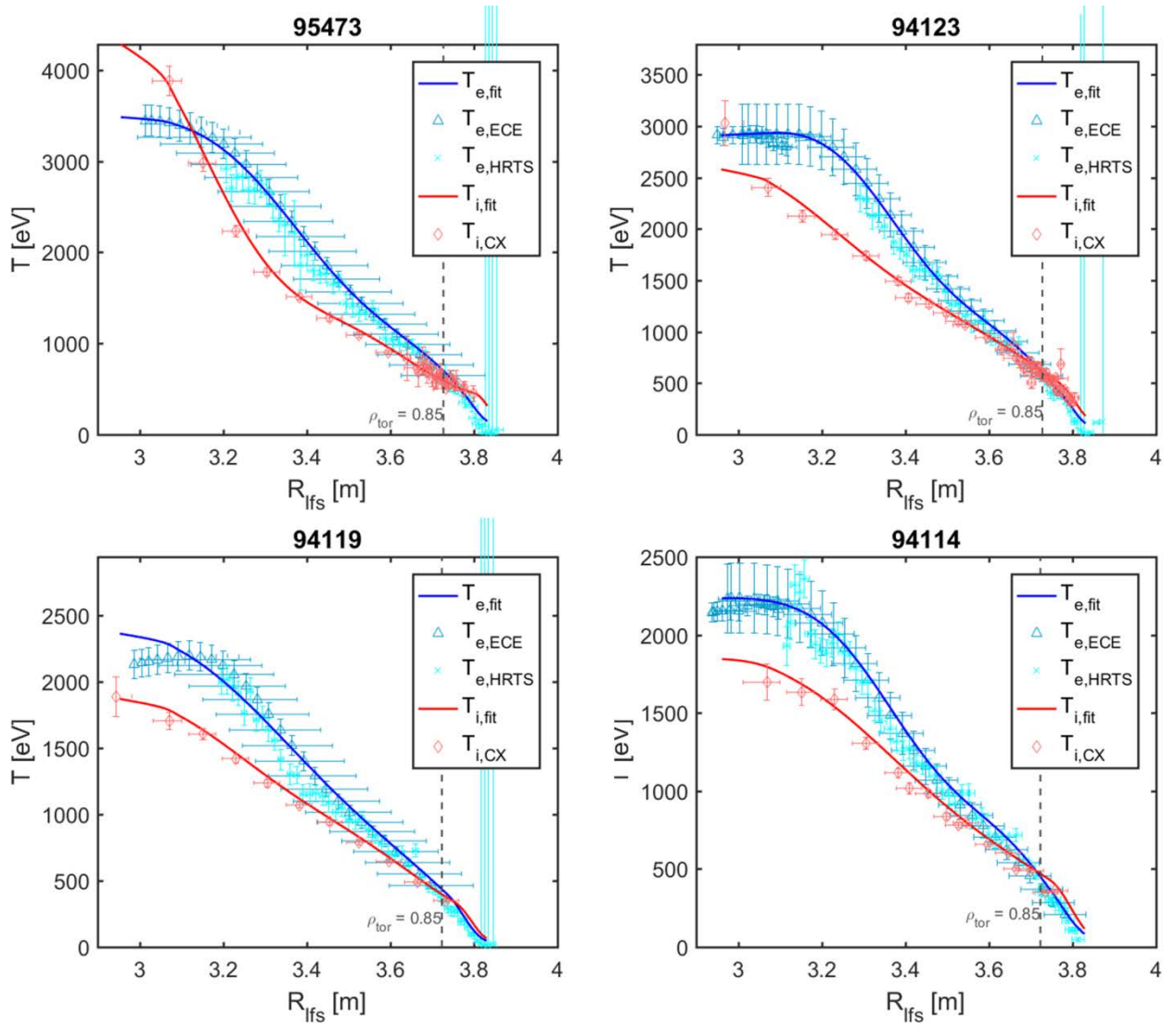


Figure 3: Electron and ion temperature profiles of the pulses analysed before the L-H transition versus JET major radius in the low field side of the torus. Equipartition power boundary condition at $\rho_{tor} = 0.85$ is reported.

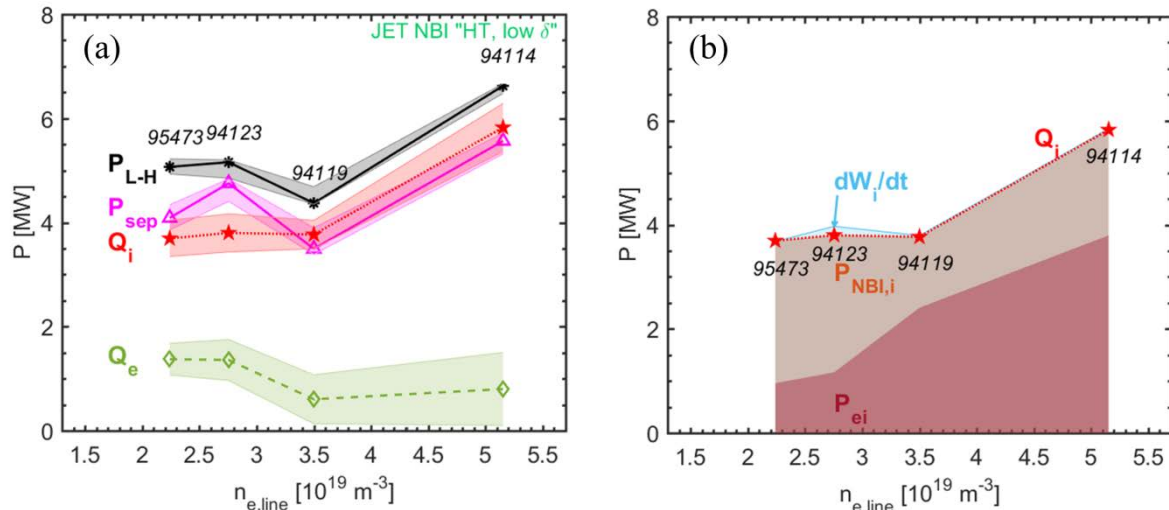


Figure 4: Power contributions for H-mode access at the transition time, as function of line-averaged density (a), showing the threshold power P_{L-H} , the radiation-corrected value P_{sep} and ion and electron power threshold Q_i and Q_e . In (b), the terms contributing to Q_i are shown.

The result of the power balance analysis at L-H transition is reported in fig. 4(a). The trend of P_{L-H} is not modified when subtracting plasma radiation: the data shows a clear minimum also in P_{sep} . Looking to the ion channel, Q_i at the L-H transition shows a clear change of slope below $n_{e,min}$. Fig. 4(b) depicts the magnitude of the terms contributing to Q_i . The impact of the time-derivative of plasma energy content is almost negligible, and Q_i is dominated by the NBI power coupled to ions $P_{NBI,i}$ at low density, and by the equipartition power $P_{ei} \propto n_e \cdot n_i$ at higher densities. Not only density is acting to increase P_{ei} : in higher-density pulses 94119 and 94114 the NBI power coupled to electrons reaches $P_{NBI,e} \sim 55 - 60 \%$, with respect to $P_{NBI,e} \sim 30 - 40 \%$ of the other 2 pulses. Strong electron NBI heating likely enhance electron-ion temperature difference, contributing to larger P_{ei} . The equipartition power is always in favour of ions (i.e. positive), due to the larger electron temperature as seen in profiles in fig. 3. The only partial exception is the low-density pulse 95473 (see fig. 3), where $T_i > T_e$ in the core region characterized although by a very small volume, not influencing the sign of the volume-integrated equipartition power. The L-H transitions analysed result having a larger ion heat flux, being $Q_i > Q_e$ throughout density branches. As illustrated in the appendix, QuaLiKiz [43] model in JETTO predicts larger T_e than T_i as observed experimentally, confirming that the ion heat transport is larger than the electron heat transport.

Regarding error estimation for ion heat fluxes, most of the concern is about the volume integrated equipartition power, where the uncertainties from density and temperatures profile measurements may result in large P_{ei} variations. In order to have an estimate on errors, we performed an additional analysis using a Gaussian process regression (GPR) method [44]. These uncertainties have been then properly propagated through the equation for the heat exchange between electrons and ions and volume integrated until $\rho_{tor} = 0.85$. An average error of 7% resulted for the calculated equipartition power at this radial location. The estimated errors on P_{ei} are used to produce the shaded error bands in fig. 4(a) for Q_i and Q_e . We have then considered a 10% error on radiation power for P_{sep} , on NBI absorbed power and on ohmic power, similarly to what assumed in previous other works [45]. Errors in plasma equilibrium reconstruction cannot be estimated and are not considered here.

4. Comparison to other tokamaks

The physics underlying the L-H transition is still not fully understood, although extensively described experimentally. Studies of L-H transitions in radio frequency (RF) heated pulses on AUG [46] and C-Mod [3] tokamaks showed that, in the density region where P_{L-H} exhibits a minimum, the power coupled to the ions Q_i increases linearly with density [47], [48], [49], [50], [51]. It is proposed that the role of the edge ion heat flux would explain the non-monotonic density dependence of the L-H threshold power and $n_{e,min}$ presence through the equipartition power between electrons and ions. Other studies are based more on the turbulence nature of the L-H transition, happening as a consequence of the stabilization of plasma turbulence by a radial electric field shear [52]. Likely these phenomena are correlated, since the equipartition power changes the T_i/T_e ratio and hence affects the turbulence drive and/or vice-versa. In AUG-based theory, such a key role of ion heat channel in triggering L-H transition is expected since the L to H transition is thought as a result of the competition between the $\vec{E} \times \vec{B}$ shear and the turbulence driven transport. A larger ion temperature does reinforce the $\vec{E} \times \vec{B}$ shear via the main

diamagnetic velocity $\mathbf{v}_{dia} = \frac{\nabla p_i}{en}$ (being p_i the ion pressure and n the plasma density). Recent analyses on AUG do indeed link the turbulence nature of L-H transition with the importance of the ion channel and therefore the ion heat flux at the transition [53]. Therefore, one expects an increase of the power necessary to enter in H mode as the power coupled to the ions is reduced, as observed in RF dominantly heated pulses in AUG and C-Mod. Nonetheless, for AUG pulses heated only by Neutral Beam Injection (NBI), a minimum in density for the power coupled to the ions was still present [49].

A relation based on a regression from AUG and C-Mod data for the sufficient edge ion heat flux per unit of plasma surface ($q_i = Q_i / S$) has been proposed in [51]:

$$q_{i,fit}^{LH} = 0.0021 \bar{n}_e^{1.07 \pm 0.09} B_T^{0.76 \pm 0.2} \text{ [MW/m}^2\text{]} \quad (\text{eq. 5})$$

We represent in fig. 5 the data of AUG, C-Mod and JET versus the proposed ion heat flux scaling $q_{i,fit}$. For JET we have considered Q_i results obtained in section 3 (labelled as “JET NBI HT, low δ ”) and ion heat fluxes estimated for 2 other sets of data regarding NBI-heated L-H transitions with same plasma parameters except plasma shape and density (“JET NBI HT, high δ ” and “JET NBI VT”). Details on these 2 supplementary datasets are given in the appendix A, in addition to details already presented in [22], [23], [24]. If we look to (NBI-only) JET data (fig. 5) we see that they mostly depart from the proposed scaling. It is interesting to note that AUG NBI-only pulses [49] also depart from the proposed scaling. The deviation of NBI-heated transitions is evident when trying to include them in the scaling law (eq. 5), with a corresponding RMSE increase of $\sim 50\%$.

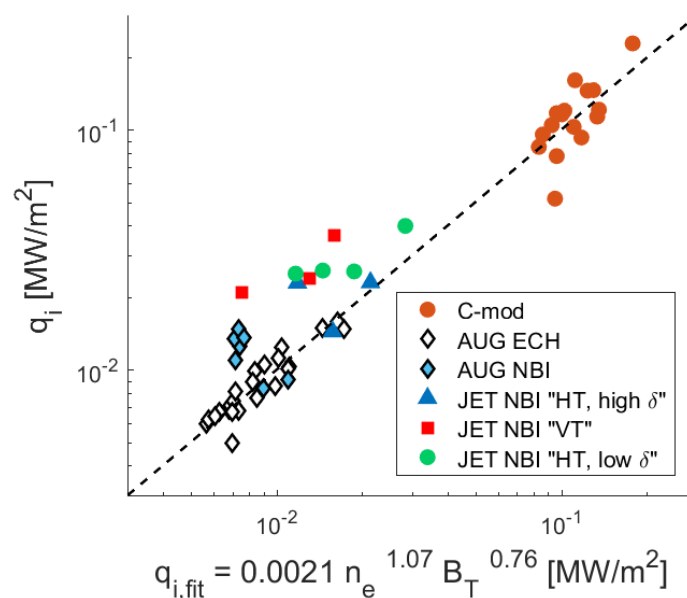


Figure 5: Comparison the observed ion heat flux per unit of plasma surface q_i at L-H transition to the scaling ($q_{i,fit}$) proposed in [51] derived from AUG and C-mod RF-heated plasmas. The figure includes NBI-heated transitions from AUG [49], and JET as presented in section 3 – labelled as “JET NBI HT, low δ ” - and in the appendix A for “JET NBI HT, high δ ” and “JET NBI VT” [22], [23], [24].

P_{L-H} has been already shown to depend on toroidal rotation [54], [55], and NBI input torque can indeed play a role on the threshold. Regarding our analysis, it is however impossible to disentangle the impact of the induced toroidal rotation and density on P_{L-H} and Q_i since they simultaneously vary in each pulse, and there is not a clear dependence of P_{L-H} on plasma rotation in the dataset analysed. NBI input torque though may not be the unique difference with respect to RF-heated plasmas. Even at zero torque, different P_{L-H} resulted in NBI-heated vs plasmas heated by electron cyclotron resonance heating ECRH in DIII-D [55]. When comparing NBI to RF pulses, some differences can be identified as key player in the L-H transition thought as a result of the competition between the $\vec{E} \times \vec{B}$ shear and the turbulence driven transport. As said, NBI is accompanied by a co-torque and hence larger \mathbf{v}_ϕ , reducing the $\vec{E} \times \vec{B}$ shear. Second, the fraction of ion heating is generally larger in NBI pulses than in ICRH or ECRH heated plasmas, influencing the equipartition term as well as the turbulence drive. In [49], \mathbf{v}_ϕ is hypothesised as a possible explanation for the non-monotonic L-H power threshold curve. Concerning

the turbulence drive, Resistive Ballooning Modes (RBM) are destabilized as T_i/T_e increases [52], while ITG modes are stabilized by larger T_i/T_e [56]. Therefore, on the low density branch, at lower resistivities, lower T_i/T_e obtained in RF heated pulses could be destabilizing, explaining qualitatively the need for more power to enter H mode. At higher densities and higher resistivities, on the contrary, larger T_i/T_e could lead to more unstable RBM modes, hence the need for more power as T_i/T_e increases, as proposed in [52].

Concerning the role of equipartition, a phenomenological model for P_{L-H} threshold that recovers a minimum in density has been proposed in [57]. It identifies the power carried by ions, Q_i , and the equipartition power, P_{ei} , as critical actors in determining the power threshold, following the findings of AUG experiments. The ratio of the two quantities is defined as $\Pi_{ei} = \frac{P_{ei}}{Q_i}$. Π_{ei} is found to be ≈ 1 in case of dominant electron heating (as AUG ECRH plasmas) and ≈ 0 for dominant ion heating; it can also be negative in case of $T_i > T_e$ and hence negative P_{ei} . Making use of the L-mode scaling law for the energy confinement time, τ_{th} (required for the whole plasma and separately for electron and ion species), P_{L-H} is found to be:

$$P_{L-H} \approx \left(\mathbf{1} - \frac{\Xi_{ei} T}{n_e^{2.3}} Q_i \right)^{-1} \left(\mathbf{1} + \frac{\tau_{th,i}}{\tau_{th,e}} \right) Q_i \quad (\text{eq. 6})$$

where $\Xi_{ei} \propto \Pi_{ei}$ and $\mathbf{T} \propto P_{loss}^{3/2} \bar{n}_e^{-5/2} \tau_{th}^{1/2}$ (for the definitions of all the terms refer to [57], where $P_{L-H,i} = Q_i$ and $P_{loss} = P_{L-H}$). P_{L-H} from eq. 6 admits a minimum only if $\Pi_{ei} \geq 0$, predicting the absence of $n_{e,min}$ in case of dominant direct ion heating. In light of the later model, JET data presented in section 3 fall in the case of strong, although not dominant, ion heating, with positive Π_{ei} .

In order to apply this phenomenological model to our JET study, we cannot evidently use the Q_i linear relation in density (eq. 5) based on AUG and C-mod experimental findings [51], as the model would suggest. Eq. 5 does not apply indeed to NBI-heated JET plasmas, as already discussed, and it would lead to huge discrepancies in predicted P_{L-H} . Instead, if we take Q_i from our analysis, and we estimate all the parameters necessary for eq. 6 from our transport modelling, we can verify the model law for our JET data. We find a surprisingly good agreement in P_{L-H} , as depicted in fig. 6. On the other side, the estimation of all the parameters for eq. 6 is in fact complex. For the plasmas analysed, beside plasma kinetic profiles, the model requires estimating a profile shape parameter to take into account the differences between volume and line averages of radial profiles. Moreover, electron/ion energy confinement times have been estimated making use of the results of the power balance analysis. The detailed information needed for the model makes the phenomenological law difficult to use for a large database unless using statistical approximations of parameters as done for AUG case. Then, if q_i relation in eq. 5 does not hold (e.g. for NBI-heated plasmas), Q_i must be estimated through a power balance analysis similar to the one presented in this paper. These constraints limit the predictive strength of the model, although the model is here formally verified with JET data.

5. Conclusion and outlook

In this work, we presented the first power balance analysis at the L-H transition time of a set of dedicated NBI-heated deuterium experiments, with the aim of identifying the different power terms contributing to the transition and estimating separately ion and electron power channels.

Thanks to a density scan, we identified density branches of P_{L-H} , with the identification of the $n_{e,min}$ region where P_{L-H} exhibits a minimum in density. Through transport modelling, we have then estimated the edge, surface-integrated, ion heat flux Q_i at the last L-mode instant before the transition. The resulting Q_i shows a clear change of slope below $n_{e,min}$. At low-density, the NBI power largely contributes to Q_i , while at higher density the equipartition power increases and become dominant. We have noted that, in almost all the analysed cases, $T_e > T_i$ throughout the whole plasma core region, while $T_e \approx$

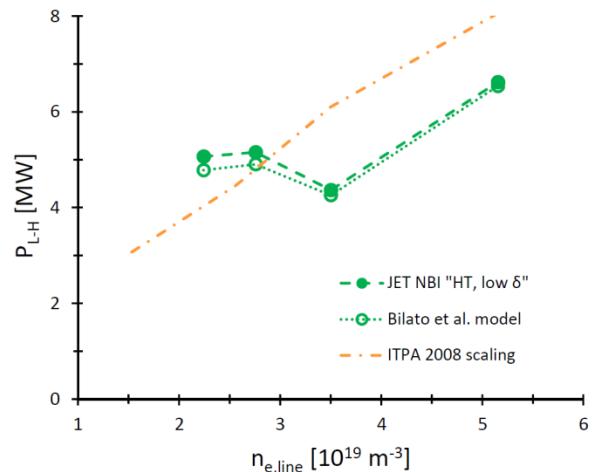


Figure 6: Comparison of JET data to the L-H transition phenomenological model presented in “Bilato et al.” [57]. The ITPA 2008 scaling is also reported. P_{L-H} in Bilato et al. model has been estimated using Q_i from our power balance analysis and not from AUG + C-mod scaling [51].

T_i within experimental error bars at the edge. Although Q_i results larger than the power coupled to electrons Q_e , core $T_e > T_i$ is explained by the dominance of ion energy transport in plasma core, confirmed by quasilinear gyrokinetic transport modelling with QuaLiKiz code.

For both AUG NBI heated pulses [49] and JET NBI heated pulses, a minimum in density or at least a clear change in the L-H threshold power with respect to density remains, even when only the power coupled to the ions is plotted against density, in contrast to the reported monotonic ion heat flux as the density decreases in RF dominantly heated pulses in AUG and C-Mod [49], [51]. The presence of $n_{e,min}$ cannot be explained in our case by the ion heat flux and equipartition power throughout density branches. NBI versus RF heated plasmas present indeed various differences, higher v_ϕ for NBI pulses impacting the $\vec{E} \times \vec{B}$ shear, larger T_i/T_e impacting the turbulence drive and finally larger $(T_i - T_e)$ impacting the equipartition contribution. To account for all these effects, integrated modelling is required, including NBI power/torque deposition as well as a validated turbulent transport model up to the LCFS in L-mode edge. Work is still ongoing in validating quasilinear turbulence models such as QuaLiKiz and TGLF in the L-mode edge region (see for example [58], [59]).

In the meanwhile, the recent phenomenological model proposed in [57] for AUG has been applied to JET cases. The model has been developed using the linearity of Q_i in density observed in AUG, which is not valid for the JET case presented here. Using instead Q_i values from the power balance analysis, the model reproduce with good agreement the non-monotonical behaviour of P_{L-H} in density. Alas, the detailed information required for P_{L-H} estimation and the invalidity of AUG + C-mod scaling for Q_i (eq. 2) for our JET NBI pulses make the applicability of the model limited for a larger database and predictions.

By the data being collected with plasmas of different isotopes at JET [19], it will be then possible to evaluate the isotope effect on the L-H transition power balance. Improving the understanding of the physics of L-H transition can benefit from both experimental and theoretical side. Detailed experimental measurements and analyses, such as on the radial electric field, are also fundamental to interpret L-H transition findings [60], [61]. On the other hand, gyrokinetic modelling can help in the understanding of the theory of L-H transition, in particular regarding the turbulence characteristics right before the H-mode transition. Finally, integrating validated reduced turbulence models, while accounting properly for the NBI induced toroidal velocity should allow us to progress towards predictive physics based L-H transition models [62].

Appendix A: supplementary datasets

We present in this appendix some details on the two supplementary datasets of JET-ILW experiments used in section 4 for fig. 5. The data comes from density scans in NBI-heated, D plasmas at $B_t = 3$ T, $I_p = 2.5$ MA and Z_{eff} within 1.1 and 1.6 [22], [23], [24]. All the settings were similar to pulses presented in sec. 2, except the plasma shape. Plasma shape has already been shown to affect P_{L-H} and $n_{e,min}$ in JET, as described in e.g. [27]. The first supplementary set is the ‘‘vertical target’’ divertor configuration dataset (‘‘JET NBI VT’’ in fig. 5), which is characterized to have plasmas with both inner and outer strike points on vertical target tiles, while the second supplementary set, ‘‘JET HT, high δ ’’, has the same divertor configuration of the data presented in section 2, except a larger triangularity value. These data have been collected in previous experimental campaigns, before the recent improvement of main-ion CX spectroscopy diagnostic, which allows measuring core ion temperature. Alas, first operations of JET with the ITER-like wall led to difficulties in the interpretation of core ion temperature measurements by Charge-Exchange (CX) spectroscopy of the Carbon CVI line [63]: a reduction by a factor of ten in carbon concentration was observed, while new impurities, notably Tungsten (W), led to additional spectral lines in the CX region of interest. This issue affected also the two supplementary datasets, causing a lack of core T_i measurement. T_i profile is although necessary to perform a power balance analysis. For ‘‘JET NBI VT’’ and ‘‘JET HT, high δ ’’, core T_i has been therefore predicted by the quasilinear gyrokinetic transport model QuaLiKiz [64], [43]. QuaLiKiz is embedded in the transport modelling platform JETTO [65]. JETTO-QuaLiKiz has been lately used to simultaneously predict ion and electron temperatures as well as electron density evolution. In other JET pulses with available core T_i CX measurements, QuaLiKiz-JETTO predicted profiles were shown to agree with measurement within error bars [43], [66], up to the pedestal region. In [67] the simultaneous profile evolution over 10 confinement times reproduced successfully all measured profiles (electron and ion temperatures, electron density and toroidal rotation) within uncertainties and allowed therefore the prediction of W accumulation similarly to the experiment.

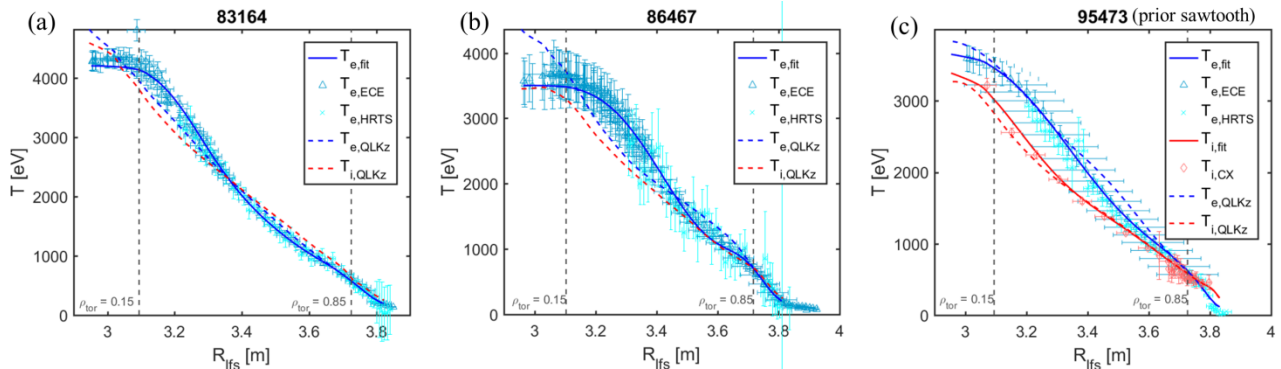


Figure 7: Examples of QuaLiKiz temperature predictions (“ T_{QLKz} ”) in both electron and ion channels, compared to available measurements (fitted profiles “ T_{fit} ”). Fig. (a) and (b) represents respectively cases for “HT, high δ ” (pulse 83164) and “VT” (pulse 86467) datasets, at the transition time $t_{\text{L-H}}$. Fig. (c) refers to pulse 95473 “HT, low δ ” dataset (see sec.2), at a time instant before the arrival of a sawtooth drop.

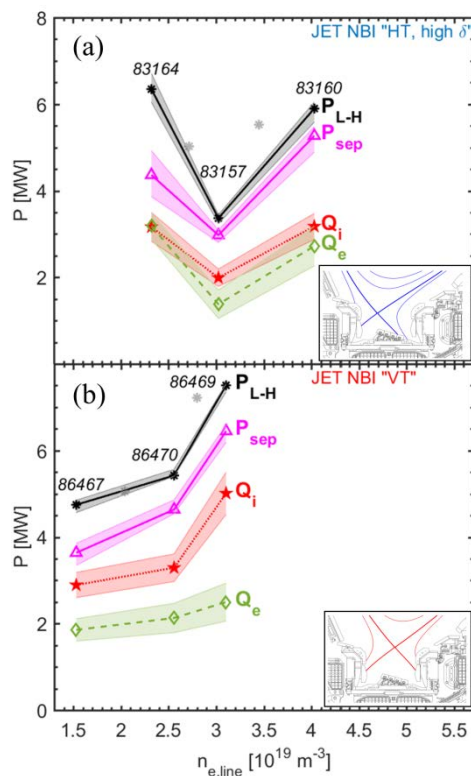


Figure 8: Power contributions for H-mode access at $t_{\text{L-H}}$, as function of line-averaged density for a) “HT, high δ ” and b) “VT” datasets.

In this work, QuaLiKiz predictions are trustworthy outside $\rho_{\text{tor}} = 0.15$: inside it the heat transport is dominated by MHD activity, in particular by sawteeth, which are not modelled in the present work. Since in our analysis we are considering volume-integrated quantities contributing to $P_{\text{L-H}}$, the plasma volume in the central region is small enough (2-3% of the total plasma volume lies within $\rho_{\text{tor}} < 0.15$) to make any discrepancy in central temperature negligible. In order to validate the modelling procedure, the QuaLiKiz predicted electron temperature (constrained by boundary conditions at $\rho_{\text{tor}} = 0.85$) is compared to measurements. Moreover, T_i profile has been predicted also for “HT, low δ ” dataset presented in sec. 2, where a comparison with the available core T_i measurements is possible, to further validate the prediction. Figs. 7(a) and 7(b) presents two example pulses of respectively “HT, high δ ” and “VT” datasets, where core T_i measurement is missing. These figures show the reconstructed T_i profiles at L-H transition, together with T_e profile from measurements and QuaLiKiz prediction. The prediction in the electron channel agrees with measurements within error bars, with some discrepancy inside $\rho_{\text{tor}} \approx 0.15$ for fig. 7(b). Fig. 7(c) shows QuaLiKiz temperature profile reconstruction in electron and ion channels just before the arrival of a sawtooth drop for pulse 95473 of the “HT, low δ ” dataset: the prediction agrees with the measurements all over the plasma volume. We have then used the predicted core T_i profiles to perform a power balance analysis for “HT, high δ ” and “VT” datasets, with the method illustrated in sec. 3. The results are shown in details in fig. 8, and Q_i estimations have been included in fig. 5. Shaded error bands of fig. 8 are calculated with the same method presented in section 2 and 3, considering similarly an average error of 7% on P_{ei} term. These results are in agreement with the dataset presented in the main paper, and strengthen the conclusion of the present work.

Acknowledgements

This work has been carried out within the framework of the EUROfusion Consortium and has received funding from the Euratom research and training programme 2014-2018 and 2019-2020 under grant agreement No 633053. This work has been supported also by an EUROfusion Engineering Grant. The views and opinions expressed herein do not necessarily reflect those of the European Commission. Additionally, the work was supported in part by Spanish Grant FIS2017-85252-R, funded by MCIN 10.13039/501100011033 and by ERDF “A way of making Europe”. The authors wish to thank C. Angioni, R. Bilato, T. Bolzonella, J. Hughes, F. Köchl, U. Plank and F. Ryter for the useful inputs and discussions. In particular, data for fig. 5 have been kindly provided by J. Hughes and F. Ryter.

References

- [1] Wagner F. et al 1982 Phys. Rev. Lett. 49 1408
- [2] Martin Y.R. et al 2008 J. Phys.: Conf. Ser. 123 012033
- [3] Greenwald M. et al., Phys. Plasmas 21, 110501 (2014)
- [4] Takizuka T. (H-mode Power Threshold Working Group) 2004 Plasma Phys. Control. Fusion 46 A227–33
- [5] Ryter F. and the H-mode Threshold Database Group 2002 Plasma Phys. Control. Fusion 44 A415–21
- [6] ITER Physics Basis 1999 Chapter 2 Nucl. Fusion 39 2175–49
- [7] Snipes J.A. et al 1996 Nucl. Fusion 36 1217
- [8] Fielding S.J. et al 1996 Plasma Phys. Control. Fusion 38 1091
- [9] Hubbard A.E. et al 1998 Plasma Phys. Control. Fusion 40 689
- [10] Carlstrom T.N. and Groebner R.J. 1996 Phys. Plasmas 3 1867
- [11] Fukuda T. et al 1997 Nucl. Fusion 37 1199
- [12] Andrew Y. et al 2006 Plasma Phys. Control. Fusion 48 479
- [13] E. Joffrin et al 2019 Nucl. Fusion 59 112021
- [14] Maggi C. et al 2014 Nucl. Fusion 54 023007
- [15] Horton L. D. et al, “Dependence of the H-mode Threshold on the JET Divertor Geometry” (Maastricht, 1999) ECA vol 23J p 193
- [16] Hillesheim J. et al, “Role of stationary zonal flows and momentum transport for L-H transitions in JET”, EX/5-2, 26th IAEA Fusion Energy Conference, Kyoto, Japan (2016)
- [17] Maggi C. F. et al., 2018 Plasma Phys. Control. Fusion 60 014045
- [18] Hillesheim J. et al, “Implications of JET-ILW L-H Transition Studies for ITER”, EX/4-1, 27th IAEA Fusion Energy Conference (FEC 2018), Gandhinagar, India (2018)
- [19] E.R. Solano et al 2022 Nucl. Fusion 62 076026
- [20] Doyle et al. Nucl. Fusion 47 (2007) S18–S127
- [21] Vincenzi P. et al. Fusion Engineering and Design 123 (2017) 473–476
- [22] Solano E. et al., “Power balance analysis at the L to H transition in JET-ILW”, 23rd Joint EU-US Transport Task Force Meeting, Seville, 2018
- [23] Vincenzi P. et al., “Ion heat channel at the L-H transition in JET-ILW”, 46th EPS conf., P2.1081, Milano, Italy 2019
- [24] Vincenzi P. et al., “Power balance analysis of JET-ILW L-H transition in Deuterium plasmas”, 4th Asia-Pacific Conference on Plasma Physics, MF1-I5, 26-31 Oct, 2020, Remote e-conference
- [25] R. Neu et al., Journal of Nuclear Materials 438 (2013) S34–S41
- [26] Solano E.R. et al, Nucl. Fusion 57 (2017) 022021
- [27] E. Delabie et al., “Overview and interpretation of L-H threshold experiments on JET with the ITER-like Wall”, EX/P5-24, 25th Fusion Energy Conference, IAEA FEC 2014 - St. Petersburg, Russian Federation
- [28] Giroud C. et al., Review of Scientific Instruments 79, 10F525 (2008)
- [29] Pasqualotto R., Review of Scientific Instruments 75, 3891 (2004)
- [30] Frassinetti L. et al., Review of Scientific Instruments 83, 013506 (2012)
- [31] Delabie E. et al., Rev. Sci. Instrum. 87, 11E525 (2016)
- [32] Hawkes N. C. et al., Review of Scientific Instruments 89, 10D113 (2018)
- [33] Sirinelli A., et al., Rev. Sci. Instrum. 81, 10D939 (2010)
- [34] Brix M. et al, Rev. Sci. Instrum. 83, 10D533 (2012)
- [35] Réfy D. I. et al., Rev. Sci. Instrum. 89, 043509 (2018)
- [36] Cenacchi G. and Taroni A. 1988 Rapporto ENEA RT/TIB(88)5
- [37] Romanelli M. et al 2014 Plasma Fusion Res. 9 3403023
- [38] Hirvijoki E. et al. 2014 Computer Physics Communications 185 1310–132

- [39] Meister H., *Rev. Sci. Instrum.*, Vol. 75, No. 10, 2004
- [40] Brix M. et al., 2008 *Rev. Sci. Instrum.* 79 10F325
- [41] Ingesson L.C. et al., *Nucl. Fusion* 38, 1675 (1998)
- [42] Ingesson L.C. et al., *Proceedings of the 24th EPS Conference on Controlled Fusion and Plasma Physics*, Vol. 21A (EPS, 1997), Part I, pp. 113 – 116
- [43] Bourdelle C. et al 2016 *PPCF* 58 014036
- [44] Ho A. et al 2019 *Nucl. Fusion* 59 056007
- [45] Ryter F. and Cavedon M., private communication
- [46] Meyer H. et al 2019 *Nucl. Fusion* 59 112014
- [47] Sauter P. et al 2012 *Nucl. Fusion* 52 012001
- [48] Ryter F. et al 2013 *Nucl. Fusion* 53 113003
- [49] Ryter F. et al 2014 *Nucl. Fusion* 54 083003
- [50] Ryter et al F. 2016 *Plasma Phys. Control. Fusion* 58 014007
- [51] Schmidtmayr M. et al 2018 *Nucl. Fusion* 58 056003
- [52] Bourdelle C. et al., *Nucl. Fusion* 55 (2015) 073015
- [53] T. Eich et al 2021 *Nucl. Fusion* 61 086017
- [54] P Gohil et al 2008 *J. Phys.: Conf. Ser.* 123 012017
- [55] McKee G.R. et al., *Nucl. Fusion* 49 (2009) 115016
- [56] Casati A. et al., *Phys. Plasmas* 15, 042310 (2008)
- [57] Bilato R. et al., *Nucl. Fusion* 60 (2020) 124003
- [58] Snoep G. et al., “GENE studies of JET-ILW L-mode edge and QuaLiKiz validation”, 2020, 24th meeting of ITPA Topical Group Transport and Confinement, Garching, Germany
- [59] Snoep G. et al., “Validation of reduced order turbulence models in the tokamak L-mode near-edge”, 2021, 25th Joint EU-US TTF Meeting, York, U.K.
- [60] C. Silva et al 2021 *Nucl. Fusion* 61 126006
- [61] Cavedon M. et al., *Nucl. Fusion* 60 (2020) 066026
- [62] Bourdelle C. et al., *Nucl. Fusion* 60 (2020) 102002
- [63] Menmuir S. et al, *Review of Scientific Instruments* 85, 11E412 (2014)
- [64] Bourdelle C. et al 2007 *Phys. Plasmas* 14 112501
- [65] Citrin J. et al, *PPCF* 59 (2017) 124005
- [66] Casson F.J. et al., 27th IAEA Fusion Energy Conference (FEC 2018), IAEA-CN-258, TH/3-2
- [67] Breton S. et al 2018 *Nucl. Fusion* 58 096003